Simulating flow around scaled model of a hypersonic vehicle in wind tunnel

T V Markova[1], A A Aksenov[1], S V Zhluktov[1], D V Savitsky[1], A D Gavrilov[1], E E Son[1] and A N Prokhorov[2]

[1] Joint Institute for High Temperatures of the Russian Academy of Sciences, Izhorskaya 13 Bldg 2, Moscow 125412, Russia
[2] Baranov Central Institute of Aviation Motors Development, Aviamotornaya Street 2, Moscow 111116, Russia

E-mail: markova@flowvision.ru

Abstract. A prospective hypersonic HEXAFLY aircraft is considered in the given paper. In order to obtain the aerodynamic characteristics of a new construction design of the aircraft, experiments with a scaled model have been carried out in a wind tunnel under different conditions. The runs have been performed at different angles of attack with and without hydrogen combustion in the scaled propulsion engine. However, the measured physical quantities do not provide all the information about the flowfield. Numerical simulation can complete the experimental data as well as to reduce the number of wind tunnel experiments. Besides that, reliable CFD software can be used for calculations of the aerodynamic characteristics for any possible design of the full-scale aircraft under different operation conditions. The reliability of the numerical predictions must be confirmed in verification study of the software. The given work is aimed at numerical investigation of the flowfield around and inside the scaled model of the HEXAFLY-CIAM module under wind tunnel conditions. A cold run (without combustion) was selected for this study. The calculations are performed in the FlowVision CFD software. The flow characteristics are compared against the available experimental data. The carried out verification study confirms the capability of the FlowVision CFD software to calculate the flows discussed.

1. Introduction

After the design of the experimental hypersonic vehicle has been determined, experiments with a scaled model of the vehicle have been carried out in a wind tunnel. The runs proceeded at different angles of attack without burning hydrogen in the combustion chamber of the model and with burning. Numerous publications are dedicated to hypersonic flows. The physical phenomena accompanying such a flow and different mathematical models describing these processes are discussed in detail in monograph [1]. The goals of the given work are twofold: numerical investigation of the flow around the scaled HEXAFLY model in the wind tunnel and verification of the FlowVision software. The peculiarity of the numerical statement of the problem is that the computational domain is bounded by the walls of the wind tunnel duct, the external and internal surfaces of the model as well as by the surface of the holder. Hence, the calculations of the flow past the model take into account the effects of the wind tunnel walls and the model holder. A cold run (without hydrogen combustion) is simulated. Since the Mach number developed in the wind tunnel is relatively low (about 7), a simplified model of the physical

processes is used in the calculations discussed. The model does not allow for nonequilibrium chemical reactions in the high-temperature regions. The computed aerodynamic characteristics of the model are compared against the available experimental data. The agreement is good, therefore, the FlowVision software can be used for calculations of the flow around the full-scale vehicle under real flight conditions.

2. Mathematical model

The following equations are integrated in the FlowVision software. The continuity equation:

$$\frac{\partial \rho}{\partial t} + \nabla(\rho \vec{V}) = 0, \tag{1}$$

here t is time, ρ is the fluid density, $\vec{V}$ is the flow velocity. The momentum equation:

$$\frac{\partial \rho \vec{V}}{\partial t} + \nabla(\rho \vec{V} \otimes \vec{V}) = -\nabla p + \nabla \hat{\tau}_{\text{eff}} + \rho \vec{g}, \tag{2}$$

$$(\vec{V} \otimes \vec{V}) = \begin{pmatrix} V_{xx} & V_{xy} & V_{xz} \\ V_{yx} & V_{yy} & V_{yz} \\ V_{zx} & V_{zy} & V_{zz} \end{pmatrix}, \quad \hat{\tau}_{\text{eff}} = (\mu + \mu_t)\left(2\hat{S} - \frac{2}{3}(\nabla \vec{V})\hat{I}\right),$$

where p is the static pressure, $\vec{g}$ is the gravity acceleration, $\hat{\tau}_{\text{eff}}$ is the effective shear stress tensor, μ is the dynamic coefficient of viscosity, μ_t is the dynamic coefficient of turbulent viscosity, $\hat{S}$ is the deformation rate tensor, $\hat{I}$ is the unit tensor. The energy equation:

$$\frac{\partial(\rho H)}{\partial t} + \nabla(\rho \vec{V} H) = \frac{\partial p}{\partial t} + \rho \vec{V} \vec{g} - \nabla \vec{J}_q + \nabla(\hat{\tau}_{\text{eff}} \vec{V}), \tag{3}$$

$$H = h + \frac{1}{2}\vec{V}^2, \quad h = h_0(298.15) + \int_{298.15}^{T} C_p(T)dT, \quad \vec{J}_q = -\left(\lambda + \frac{\mu_t C_p}{Pr_t}\right)\nabla T,$$

where H is the total enthalpy, $h_0(298.15)$ is the enthalpy of formation of the working fluid at 298.15 K, $C_p(T)$ is the specific heat at constant pressure, T is the absolute static temperature, $\vec{J}_q$ is the specific heat flux, λ is the coefficient of thermal conductivity, Pr_t is the turbulent Prandtl number.

System (1)–(3) is completed by the ideal gas state equation and the equations for the turbulent characteristics. "Standard' k–ε turbulence model [2] is used in the current calculations. The equations and algebraic expressions describing the model are as follows:

$$\frac{\partial(\rho k)}{\partial t} + \nabla(\rho \vec{V} k) = \nabla\left(\left(\mu + \frac{\mu_t}{\sigma_k}\right)\nabla k\right) + P_k + G_k - \rho\varepsilon(1 + \xi[\max(M_t^2, M_{t0}^2) - M_{t0}^2]), \tag{4}$$

$$\frac{\partial(\rho \varepsilon)}{\partial t} + \nabla(\rho \vec{V} \varepsilon) = \nabla\left(\left(\mu + \frac{\mu_t}{\sigma_\varepsilon}\right)\nabla \varepsilon\right) + \frac{\varepsilon}{k}(C_{\varepsilon 1}[P_k + G_k] - C_{\varepsilon 2}\rho\varepsilon), \tag{5}$$

$$\mu_t = \rho C_\mu \frac{k^2}{\varepsilon}, \quad P_k = \mu_t\left(S - \frac{2}{3}(\nabla \vec{V})^2\right) - \frac{2}{3}\rho(\nabla \vec{V})k, \quad G_k = \mu_t \frac{\beta}{Pr_t}\vec{g}\nabla T,$$

$$S = 2\sum_{i,j} S_{ij}S_{ij}, \quad S_{ij} = \frac{1}{2}\left(\frac{\partial V_i}{\partial x_j} + \frac{\partial V_j}{\partial x_i}\right),$$

here x_i is a Cartesian coordinate, V_i is the i-th component of velocity, k is the turbulent energy, ε is its dissipation rate, β is the coefficient of thermal expansion, a is the speed of sound, $C_\mu = 0.09$ is a fixed model constant. The default values of the other model constants are as follows:

$$\sigma_k = 1, \quad \sigma_\varepsilon = 1.3, \quad C_{\varepsilon 1} = 1.44, \quad C_{\varepsilon 2} = 1.92, \quad \xi = 1.5, \quad M_{t0} = 0.25. \tag{6}$$

Constants ξ and M_{t0} define the model accounting for the fluid compressibility. The above-mentioned values define the Wilcox model. Values $\xi = 1$, $M_{\mathrm{t0}} = 0$ define the Sarkar model. Both models are discussed in [2]. Note that in FlowVision, a user can specify arbitrary values of constants (6).

Computations were performed on relatively coarse grids. For this reason, FlowVision model of wall functions [3] was used in the cells adjacent to solid boundaries.

3. Numerical method

The FlowVision software allows a user to calculate different flows of gases and liquids in complex 3D domains. Numerical integration of the governing equations is based on the finite volume approach. FlowVision contains an automatic grid generator. This is an important advantage of the software, since in most CFD codes manual building a computational grid takes up to 90% of flow simulation time.

Another important advantage of FlowVision is the sub-grid geometry resolution (SGGR) method developed for generation of computational cells near curvelinear boundaries of the computational domain. The method assumes natural truncation of a hexahedral cell by a triangulated curvelinear boundary followed by Boolean subtraction of the volume found outside the domain from the parent cell. In doing so, the boundary cell transforms to a polyhedron. Thus, the internal cells are hexahedrons, the boundary cells are polyhedrons of arbitrary shape determined by the local shape of the boundary. In all the cells, the governing equations are approximated by a high-order numerical scheme. The solution in the regions with high gradients of sought-for variables and around fine geometric features can be improved by means of automated local dynamic adaptation. Note that in FlowVision, adaptation by one level means division of a hexahedral cell (parent cell) by 8 equal cells.

A new implicit velocity-pressure split algorithm [4] is used for solving the Navier–Stokes equations. Solution of the other convection-diffusion equations, constituting the mathematical model, is synchronized with solution of the Navier–Stokes equations. The algorithm assumes using the conservative velocities at cell faces, obtained at the given time step, in the convection terms of all the convection-diffusion equations. The method is compatible with technologies of moving boundaries. Besides that, method [4] enables integration of the partial differential equations at large Mach numbers with time steps essentially exceeding the explicit time step.

The algorithm is summarized below.

Stage 1. Solve pressure equation:

$$\left(\frac{d\rho}{dp}\right)^n \frac{(p_c^{n+1} - p_c^n)}{\Delta t} + \frac{1}{\Omega_c}\sum_f \left(\rho_f^n + \left(\frac{d\rho}{dp}\right)^n (p_f^{n+1} - p_f^n)\right) V_{fn}^n S_f = \frac{\Delta t}{\Omega_c}\sum_f \left(\left(\frac{\partial p^{n+1}}{\partial n}\right)_f - \left(\frac{\partial p^n}{\partial n}\right)_f\right) S_f, \quad (7)$$

where

$$\frac{d\rho}{dp} = \left.\frac{\partial\rho}{\partial p}\right|_T + \frac{1}{\rho C_p(T)} \left.\frac{\partial\rho}{\partial T}\right|_p, \quad (8)$$

indices n and $n+1$ indicate two sequential time layers, index c indicates the value of a quantity in the cell center, index f indicates the value of a quantity at a cell face, Δt is a time step, Ω_c is the volume of a given cell, S_f is the area of a given cell face, V_{fn} is the velocity projection onto the external normal $\vec{n_f}$ to the given cell face, $\partial p/\partial n$ is the static pressure derivative along the normal.

Stage 2. Compute density ρ_c^{n+1}:

$$\rho_c^{n+1} = \rho_c^n + \left(\frac{d\rho}{dp}\right)^n (p_c^{n+1} - p_c^n) \tag{9}$$

Stage 3. Compute the normal mass velocities at the cell faces:

$$W_{fn}^{n+1} = \rho_f^{n+1} V_{fn}^n - \Delta t \left(\frac{\partial p^{n+1}}{\partial n}\right)_f + \Delta t \left(\frac{\partial p^n}{\partial n}\right)_f, \tag{10}$$

where $W_{fn}^{n+1} = \rho_f^{n+1} V_{fn}^{n+1}$ is the normal component of the specific mass flow rate at a cell face.

Stage 4. Solve the momentum equation:

$$\frac{\rho_c^{n+1}\vec{V}_c^{n+1} - \rho_c^n \vec{V}_c^n}{\tau} + \frac{1}{\Omega_c}\sum_f W_{fn}^{n+1}\vec{V}_f^{n+1} S_f + \frac{1}{\Omega_c}\sum_f (\hat{\tau}_{\text{eff}}^{n+1} \cdot \vec{n})_f S_f = -2\nabla p_c^{n+1} + \nabla p_c^n + \rho_c^{n+1}\vec{g}. \tag{11}$$

Stage 5. Solve the other convection-diffusion equations constituting the mathematical model of the flow (turbulence, energy, *etc*) using the same values W_{fn}^{n+1}.

The new split algorithm is implemented in the FlowVision CFD software in such a way that calculations at a time step (stages 1–5) can be repeated when a transient problem is solved and time accuracy is required. In doing so, temperature T^{n+1} is substituted into (8) at each such iteration.

4. Formulation of the problem in FlowVision software

The scaled model of the HEXAFLY vehicle used in the experiments is shown in figure 1. The model is mounted in a wind tunnel equipped with a conical supersonic nozzle. The entire geometry is symmetric with respect to the vertical plain passing through the axis of symmetry of the nozzle and wind tunnel chamber. This allows one to save computational resources performing calculations in a half-space. Figure 2 demonstrates the flow-through part of the wind tunnel and the HEXAFLY model installed inside it. It also shows the specified boundary conditions. Inlet to the nozzle 3 is subsonic. Here total pressure $p_0 = 64$ atm and total temperature $T_0 = 2310$ K are specified. These values correspond to the experimental conditions. The working substance is the gas mixture composed of the combustion products of methane (CH_4). Its properties (molar mass, specific heat at constant pressure, viscosity and thermal conductivity) are calculated assuming thermo-chemical equilibrium at fixed values of static pressure (p) and temperature (T) and specified as tables of T and p. The aforementioned inlet conditions provide the Mach number equal to 7 at the nozzle outlet. This is the flow which encounters the model. The supersonic outlet condition is specified behind the model at surface 4. The symmetry condition is specified at the mirror plane. The walls (surfaces 1 and 2) are assumed to be adiabatic. The non-slip condition is specified at the walls.

In the experiments, the gas mixture composed of N_2, O_2, CH_4 is supplied to the wind tunnel inlet, the mass flow rates being: $G_{N_2} = 4.864$ kg/s, $G_{O_2} = 4.701$ kg/s, $G_{CH_4} = 0.581$ kg/s. Methane completely burns in the region between the nozzle inlet and the critical section. Further the gas mixture composed of N_2, O_2, CO_2, H_2O flows through the nozzle and encounters the model. The mass fractions of the components are: $Y_{N_2} = 0.479$, $Y_{O_2} = 0.234$, $Y_{CO_2} = 0.157$, $Y_{H_2O} = 0.130$. The Mach number at the outlet from the wind tunnel nozzle is 7.

In calculations, the aforementioned mixture of gases N_2, O_2, CO_2, H_2O is supplied to the wind tunnel inlet. The mixture properties are computed assuming thermochemical equilibrium

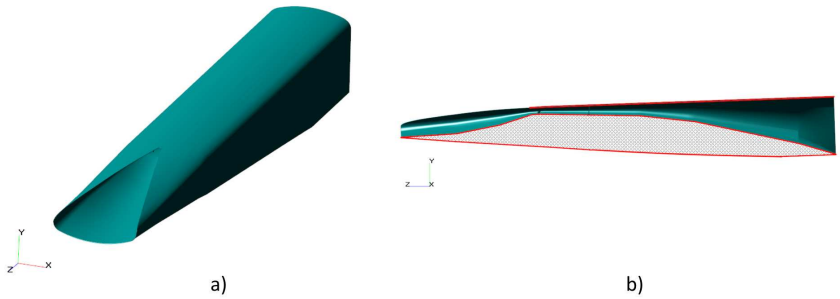

Figure 1. Scaled model of the HEXAFLY vehicle: (a) general view, (b) mirror plane section.

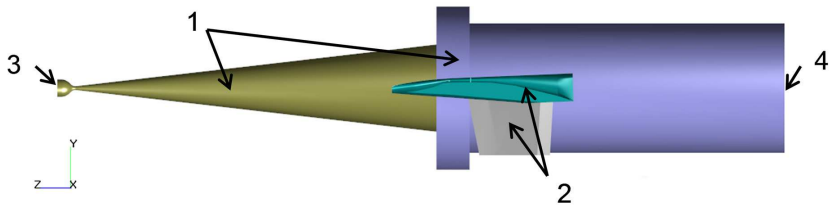

Figure 2. Boundary conditions: 1—walls of the nozzle and wind tunnel chamber; 2—walls of the HEXAFLY model and support; 3—inlet; 4—outlet.

with use of data from handbook [5]. The properties are represented as tables of static pressure and static temperature. The free stream Mach number at the forward edge of the model equals to 6.5, the corresponding flow velocity being 2400 m/s. The free stream static pressure is 630 Pa, the free stream static temperature is 330 K. The model length, width and height respectively are: 2.88 m, 0.4 m, 0.385 m. The length-based Reynolds number approximately equals to 4.3×10^6.

Apparently, not taken into account nonequilibrium effects may decrease the accuracy of the numerical predictions. However, since the free stream Mach number is relatively low, this decrease should not be essential.

Different grids were used in preliminary calculations. The results discussed below are obtained on two grids generated as follows. The initial computational grid is uniform. The size of initial cells is 0.1 m. The grid is refined in the wind tunnel nozzle and around the model. Three types of adaptation are specified: adaptation in the volume of a geometric primitive (up to the 3-rd level), adaptation near the model surfaces (4 and 8 layers of the 5-th level cells for the first and second grids respectively) and adaptation to solution around the model, viz., adaptation to the gradients of the static pressure and temperature (up to the 5-th level). Remind that in FlowVision adaptation by one level assumes division of a parent hexahedral cell by 8 equal parts and that the cells adjacent to the curvelinear boundaries of the computational domain are polyhedrons of arbitrary shape. The dimension of the first grid was limited from above by 4 million cells, the dimension of the second grid was limited by 8 million cells. As a result, the first grid built in the course of calculations contains about 3.2 million cells, the second one contains about 7.1 million cells. Figure 3 illustrates the structures of the grids around the forward part of the model and the structure of the second grid around the model and holder. The second grid better resolves the pressure field and the shocks compared to the first one.

It is worthwhile to emphasize that such a grid is variable until the steady-state solution is reached: the cells are split and merged in the course of development of solution.

The integration time step is determined by the specified CFL number:

$$\Delta t = \mathrm{CFL}\Delta t_{\mathrm{expl}}, \quad \mathrm{CFL} = 10. \tag{12}$$

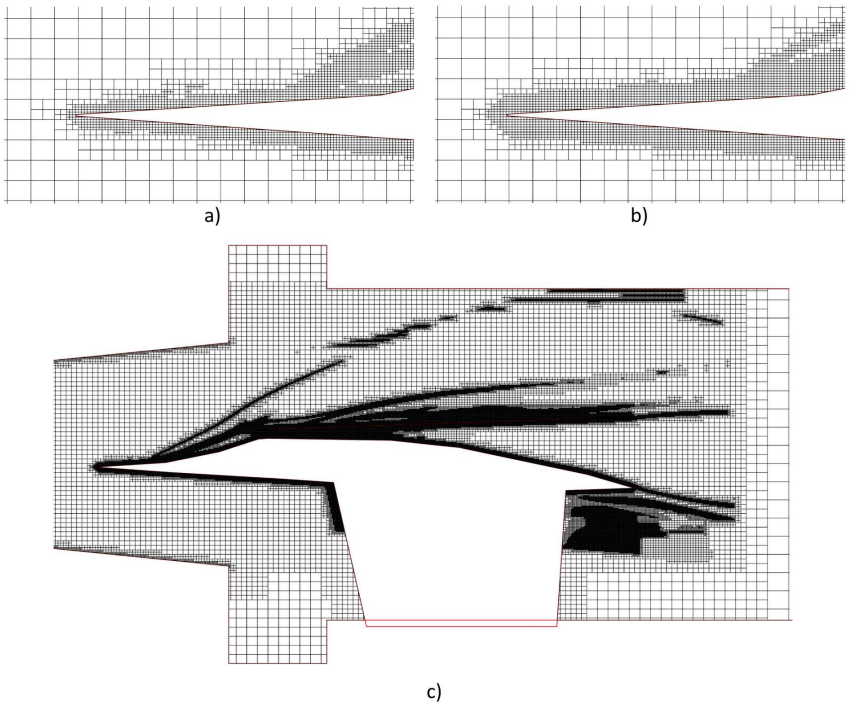

Figure 3. Computational grid: (a) first grid, adaptation around the leading edge of the HEXAFLY model (4 layers of the 5-th level); (b) second grid, adaptation around the leading edge of the HEXAFLY model (8 layers of the 5-th level); (c) second grid around the model and holder.

The explicit time step is computed as follows:

$$\Delta t_{\text{expl}} = \min_i \left(\frac{0.5 h_i}{|\vec{V}_i| + a_i}, \frac{\rho_i h_i^2}{\mu_i + \mu_{t,i}} \right), \tag{13}$$

where h_i is the size of the i-th cell, $|\vec{V}_i|$, a_i, ρ_i, μ_i, $\mu_{t,i}$ are, respectively, the velocity modulus, the speed of sound, the density, the viscosity and the turbulent viscosity in the cell center. In the calculations discussed below, time step Δt was approximately equal to 3.7×10^{-7} s.

5. Calculations

Figures 4–6 demonstrate the distributions of the Mach number, static pressure and static temperature in the mirror plane. Figure 7 shows the alignment bars of the pressure gauges installed over the model surface. The static pressure distributions along the alignment bars of the pressure gauges are shown in figures 8 and 9.

The pressure peaks observed in the figures are due to the presence of the pylon for hydrogen supply in this region. As we see, the agreement between the numerical and experimental data is good. At certain points the calculated values lay precisely on the experimental ones. Most calculated results are found within 20% band around the experimental data. In general, the computed pressure profile repeats the experimental one. However, some splashes are not reproduced by calculations. Besides that, there is a minor displacement between the profiles. There are several possible reasons for this displacement. The first reason is the triangulated geometrical model used in the calculations. Apparently, it does not precisely reproduce the shape

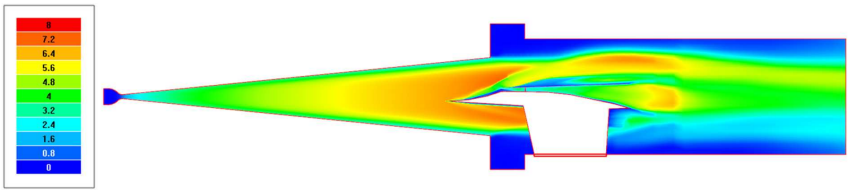

Figure 4. Distribution of the Mach number in the mirror plane.

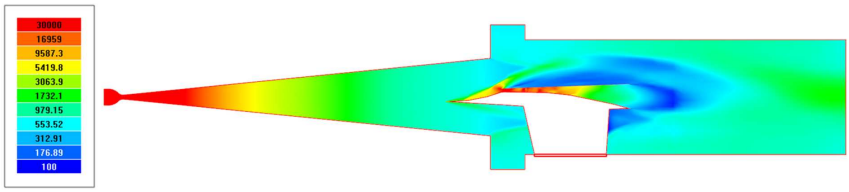

Figure 5. Distribution of static pressure in the mirror plane, Pa.

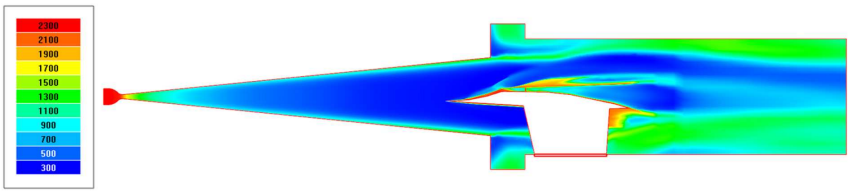

Figure 6. Distribution of static temperature in the mirror plane, K.

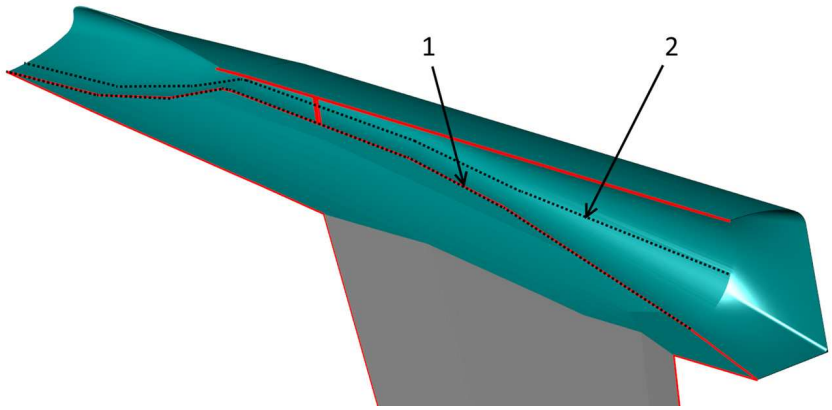

Figure 7. Arrangement of the pressure gauges over the surface of the HEXAFLY model: 1—central alignment bar of the pressure gauges; 2—side alignment bar of the pressure gauges.

of the model used in the experiment. The second possible reason consists in 3D effects which are observed in the experiments and are not taken into account in the calculations performed in a half-space. Minor disagreement between the numerical and experimental data can be produced by the simplified physical model which does not allow for non-equilibrium phenomena: as it was mentioned above, the working fluid composed of gases N_2, O_2, CO_2 and H_2O is assumed to be under thermo–chemical equilibrium. Thus, the conditions specified in the calculations, do not coincide precisely with the experimental ones. Nevertheless, the flow pattern obtained in the calculations agrees well with that observed in the experiments.

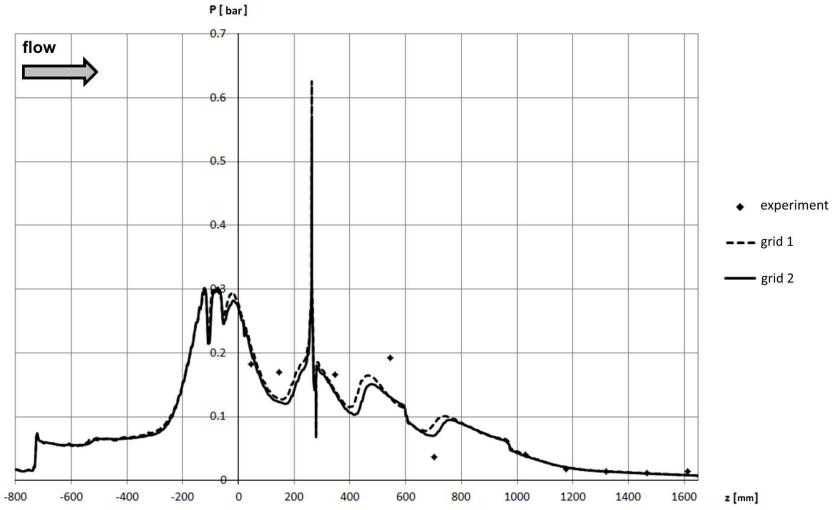

Figure 8. Distribution of static pressure along the central alignment bar of the pressure gauges, bar (line 1 in figure 7).

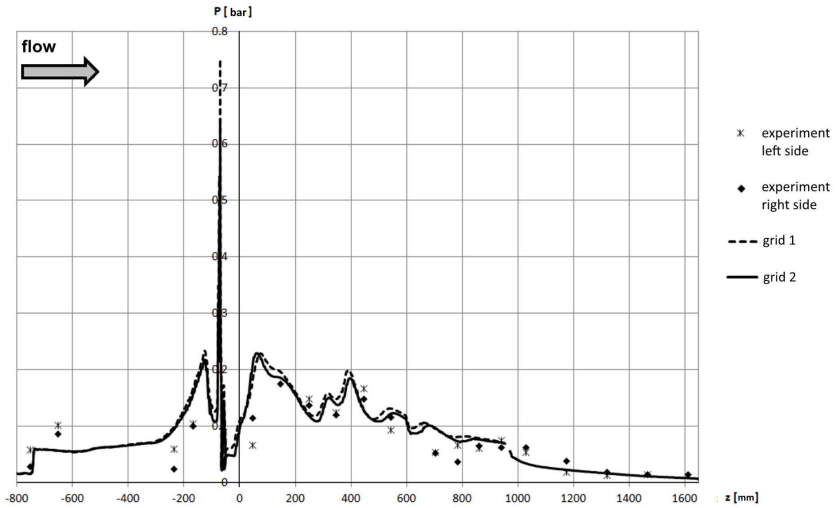

Figure 9. Distribution of static pressure along the side alignment bar of the pressure gauges, bar (line 2 in figure 7).

6. Conclusions

The work is dedicated to numerical investigation of the flow around a scaled HEXAFLY model in a wind tunnel and to verification of the FlowVision CFD software. A cold run (without hydrogen combustion) was selected for this study. The peculiarity of the study consists in taking into account the effects of the wind tunnel walls and the model holder. The calculations provided the velocity, pressure and temperature fields around and inside the HEXAFLY model. The calculations adequately reproduced the flow observed in the experiments. The agreement between the numerical and experimental data is good.

The carried out verification study indicates that the FlowVision CFD software can be used in systematic calculations of the aerodynamic characteristics of full-scale models of hypersonic vehicle HEXAFLY under different operation conditions.

Acknowledgments
This work was supported by the Ministry of Education and Science, contract No. 14.604.21.0090 since 8 July 2014, project ID: RFMEFI60414X0090.

References
[1] Lunev B B 2007 *Flow of Real Gases at High Speeds* (Moscow: FIZMATLIT)
[2] Wilcox D C 1994 *Turbulence Modeling for CFD* (DCW Industries Inc.)
[3] Zhluktov S V and Aksenov A A 2015 *Computer Research and Simulation* **7** 1221–1239
[4] Aksenov A A, Zhluktov S V, Savitskiy D V, Bartenev G Y and Pokhilko V I 2015 *J. Phys.: Conf. Ser.* **653** 012072
[5] Grigoriev I S and Meilikhov E Z (eds) 1991 *Physical Quantities: Handbook* (Moscow: Energoatomizdat)